Fermi surface of Pd_2Si

V.N. Antonov, B.Yu. Yavorsky, and V.V. Nemoshkalenko
Institute of Metal Physics, Kiev 142, Ukraine

Vl.N. Antonov, O. Jepsen, and O.K. Andersen
Max-Planck Institut für Festkörperforschung, D-70569 Stuttgart, Federal Republic of Germany

E.G. Haanappel,* M. Vosgerau, W. Joss, and P. Wyder
Max-Planck Institut für Festkörperforschung, D-70569 Stuttgart, Germany
and High Magnetic Field Laboratory, Centre National de la Recherche Scientifique, Boîte Postale 166, F-38042 Grenoble CEDEX 9, France

R. Madar and A. Rouault
Ecole Nationale Supérieure de Physique de Grenoble, Laboratoire des Matériaux et du Génie Physique, Boîte Postale 46, F-38402 Saint-Martin-d'Hères CEDEX, France

(Received 8 November 1993)

A Fermi-surface study of palladium disilicide is presented. Experimentally, the Fermi surface and the cyclotron effective masses have been studied using the de Haas–van Alphen (dHvA) effect. Theoretically, the band structure of Pd_2Si has been calculated using the linear-muffin-tin-orbital method in the atomic-sphere approximation. The Fermi surface consists of three small hole pockets, an open hole surface, and two large electron sheets. The calculated angular dependence of the extremal cross sections of the Fermi surface is in reasonable agreement with dHvA experiments. Some additional dHvA oscillations are predicted.

I. INTRODUCTION

In recent years, transition-metal silicides have been finding increasingly important applications in silicon integrated-circuit technology as, e.g., Schottky barriers, Ohmic contacts, gate electrodes, and low-resistivity interconnections. Within this family of compounds, the palladium silicides were among the first silicide compounds to be used in optoelectronic devices and in silicon technology,[1,2] for example, as buffering layers for metals. Since then they have been intensely investigated both experimentally and theoretically by a number of techniques. In particular, ultraviolet and x-ray photoemission spectroscopies,[3–5] auger-electron spectroscopy,[6,7] extended x-ray absorption spectroscopy,[7,8] electron-energy-loss spectroscopy,[9] the optical reflectivity, and ellipsometric techniques[10–12] have been used to investigate the electronic structure of the most stable phase which is the hexagonal Pd_2Si. On the theoretical side, the energy bands, the densities of states (DOS), the x-ray absorption spectra, and the total energy have been calculated using the linear-muffin-tin-orbital (LMTO) method.[13] The electronic structure and optical properties of Pd_2Si have been extensively studied in Ref. 12. Here, on the one hand, accurate measurements on high-quality single crystals of the optical response, over a wide spectral range (0.05–12 eV) with polarized light or ellipsometric techniques were performed and, on the other hand, the band structure, the l-projected DOS, the complex dielectric function, the optical conductivity, and the optical reflectivity were calculated by the LMTO method. The good agreement between experiment and theory shows that density functional theory in the local-density approximation gives a good description of the electronic states around the Fermi energy.

In the present paper, we have calculated the Fermi surface (FS) of Pd_2 Si. The band structure calculations are the same as in Ref. 12, except that we have used a very large number of **k** points in the Brillouin zone (BZ) in order to represent the Fermi surface accurately. The experimental cross-sectional areas of the FS and corresponding cyclotron effective masses were obtained using the de Haas–van Alphen (dHvA) effect. A preliminary dHvA study was reported in Ref. 14.

II. EXPERIMENT

Pd_2Si crystallizes in a hexagonal structure (space group $P\bar{6}2m$) with nine atoms per unit cell (Fig. 1). Due to the fact that the two basal planes that are displaced by $c/2$ in the c direction have different atomic sites, there are two nonequivalent Si and Pd atoms in the unit cell which have been labeled by the index (1) and (2) in Fig. 1. The measured lattice constants are $a = 6.496$ Å, and $c = 3.435$ Å,[15,16] with $c/a = 0.5285$. The Brillouin zone is shown in Fig. 2, where the symmetry points and lines are labeled in accordance with the standard notation of Ref. 17.

The Pd_2Si single crystals have been prepared using the

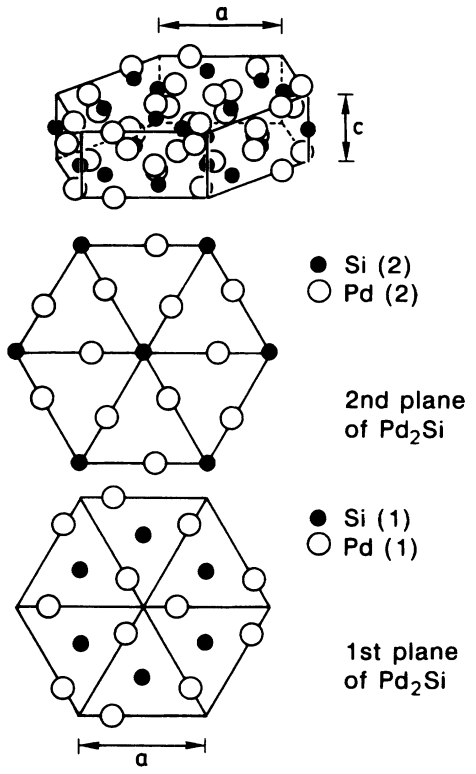

FIG. 1. Silicon and palladium atomic sites in the two alternating planes normal to the c axis and in the three-dimensional hexagonal cell in Pd_2Si. Both Si and Pd atoms are found in two nonequivalent sites, labeled (1) and (2).

modified cold crucible Czochralski method. Details of the sample fabrication have been given by Marani *et al.*[15] From the initial high-purity single crystal two rectangular samples were cut with typical dimensions $1 \times 1 \times 3$ mm^3. One sample had its longest axis parallel to the [0001] crystallographic axis, the other to the [$\bar{1}$100] axis. Samples from the same batch have also been used for measurements of resistivity and low temperature heat capacity by Laborde *et al.*[18] and for magnetoresistance measurements by Laborde *et al.*[19] The residual resistance ratio of these crystals was larger than 200.[18]

The sample was mounted in a set of tight-fitting compensated pickup coils. The assembly of sample and pickup coils could be rotated in one plane over more than $\pm 90°$ using a spiral gear rotator. The dHvA oscillations were detected using the low-frequency, large-amplitude field modulation technique with the modulation amplitude proportional to B^2 and with detection on the second harmonic. The measurements were done in a 10 T superconducting magnet with a 60 mm room temperature bore. The modulation field was provided by a water cooled resistive coil mounted in the bore of the superconducting magnet. Most measurements have been done at 4.2 K in a ^{4}He cryostat, but for the cyclotron mass measurements at five temperatures between 1.3 K and 4.2 K.

The magnetic field was always applied in a plane of high symmetry. The direction of the magnetic field in each plane was changed in 4° steps. With the two samples at our disposal, we performed measurements with the field in the (x,z) plane and the (y,z) plane for the first sample and in the (x,y) plane and the (y,z) plane for the second sample (these directions are defined in Fig. 2). Thus the (y,z) plane was measured in both samples and provided a useful check for consistency.

For the detection method used in this experiment,[20] the amplitude of a dHvA signal with frequency F at a magnetic field B is proportional to $J_2(2\pi Fb/B^2)$, where J_2 is the Bessel function of the first kind of order 2 and b is the modulation amplitude. This Bessel function has a maximum when its argument is close to π, implying that the sensitivity is largest for dHvA signals with frequency close to $B^2/2b$. Measurements done at different modulation amplitudes are more or less sensitive to different

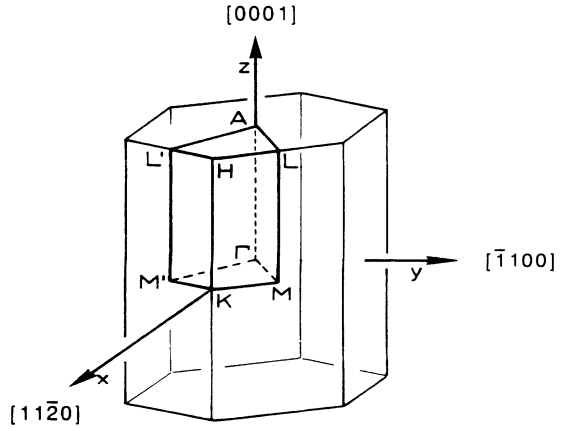

FIG. 2. The Brillouin zone of Pd_2Si and its irreducible part.

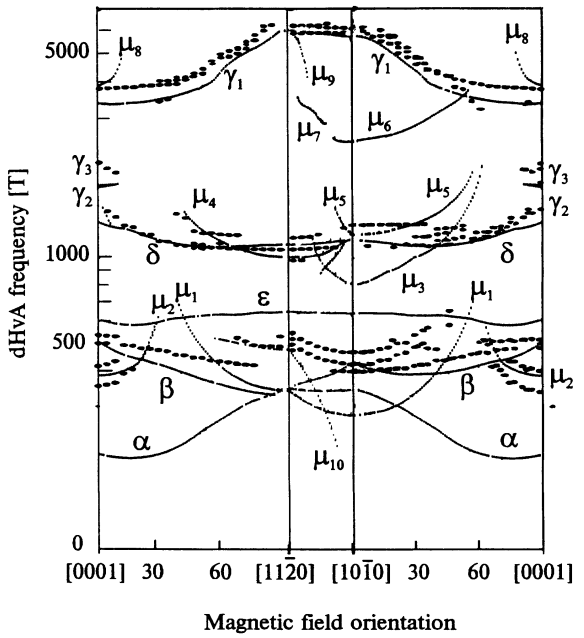

FIG. 3. Angular dependence of calculated (small dots) and measured (Ref. 14) (full dots) extremal cross sections.

dHvA frequencies. Thus it is possible to enhance certain frequencies and suppress others. To maintain a constant sensitivity for a given dHvA frequency throughout the field sweep, the modulation amplitude must be varied proportional to B^2. In Pd_2Si, the low-frequency signals (below 1500 T) have much higher amplitudes than the high-frequency signals. For each angle, two field sweeps were, therefore, performed; one with a large modulation amplitude (maximum sensitivity around 1000 T) and one with a small amplitude (maximum sensitivity around 6000 T).

The dHvA frequencies present in the signals were determined by performing a fast Fourier transform (FFT) of the data. The resolution of the FFT determines the uncertainty in the experimental value of the dHvA frequencies. In Fig. 3 this uncertainty is 2 T for the frequencies below 3000 T, and 10 T for the frequencies above 3000 T.

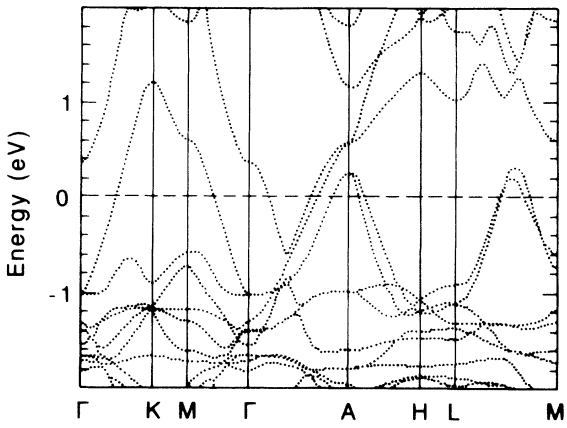

FIG. 4. Self-consistent energy band structure of Pd_2Si along the high-symmetry directions near the Fermi energy (from Ref. 12).

III. METHOD OF CALCULATION

A detailed description of the LMTO method in the atomic-sphere approximation including its application to the electronic structure of compounds, has been given elsewhere.[21,22] In the present semirelativistic calculations basis functions included angular momenta up to $l = 3$ for palladium and $l = 2$ for silicon. The "*frozen-core*" approximation was adopted and the core charge distributions were evaluated from the solutions of the Dirac equation for free atoms. Exchange and correlation contributions to both atomic and crystalline potentials were included through the local-density-functional description using the von Barth-Hedin formula.[23] The **k**-integrated functions (charge density, DOS, and l-projected DOS's) were calculated by the tetrahedron method[24] on a grid of 216 **k** points in the irreducible part of the BZ (Fig. 2). The Fermi surface and the angular dependence of the extremal cross-sectional areas were evaluated by the same method using a grid of 2366 **k** points in the irreducible part of the BZ.

IV. RESULTS AND DISCUSSION

Figure 4 shows the energy band structure of Pd_2Si near the Fermi level from Ref. 12. Four energy bands with numbers from 35 to 38 cross the Fermi energy. The states around the Fermi level are mainly of Pd d character and Si p character.[13] The band structure leads to a complicated Fermi surface, consisting of three small hole pockets, an open hole surface, and two large electron sheets. The three-dimensional (3D) computer-generated drawing of these sheets originating from different bands are presented in Figs. 5–9. They are as follows: a small hole pocket h_{35} centered at the symmetry point A (ellipsoid), another hole pocket h_{35} centered half way between M and L (the *disk*) (Fig. 5), a small hole pocket h_{36} centered at A (the *sphere*) (Fig. 6), a network of multiply connected toroidal hole-type pieces h_{36} (the rings) reflecting the hexagonal symmetry of the lattice (Figs. 6 and 7), a large electron-type surface e_{37} centered at Γ (the football) (Fig. 8), and an electron-type sheet e_{38} centered along the Γ-A direction 1/3 the distance from Γ to A (the *lens*) (Fig. 9).

Experimentally three groups of dHvA frequencies were detected, but they could only partly be associated with the band structure in Ref. 12.

In the experimental measurements the magnetic field direction was varied from [0001] to [11$\bar{2}$0], from [11$\bar{2}$0] to [$\bar{1}$100], i.e., 90°, and from [$\bar{1}$100] to [0001]. The irreducible parts of the BZ $\Gamma AHKML$ and $\Gamma AHKM'L'$

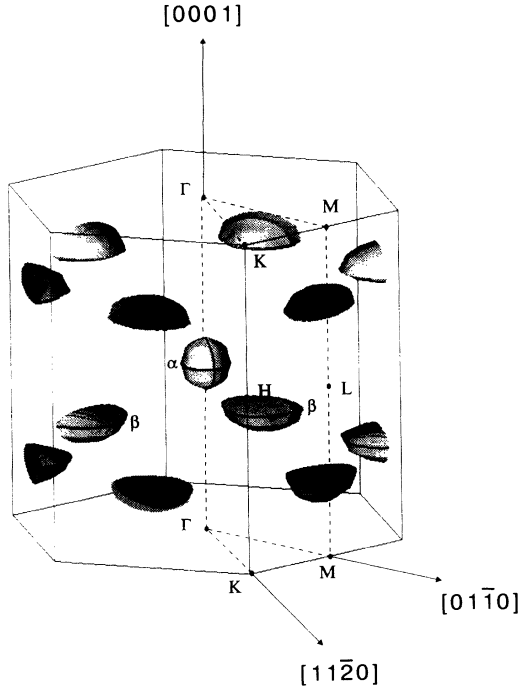

FIG. 5. The Fermi surface sheet, the ellipsoid, around the A point and the *disk* sheet in the first Brillouin zone. Greek letters denote extremal orbits on the Fermi surface of Pd_2Si.

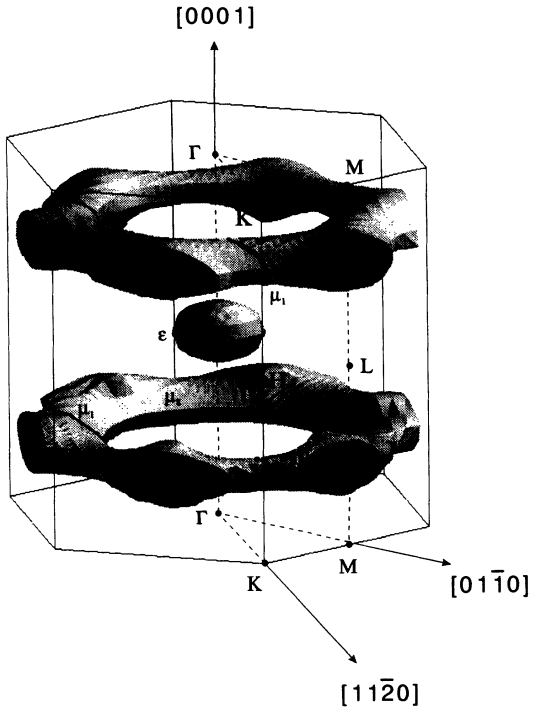

FIG. 6. The rings and the *sphere* Fermi surface sheets of Pd_2Si in the first Brillouin zone. ϵ, μ_1, and μ_8 are extremal orbits.

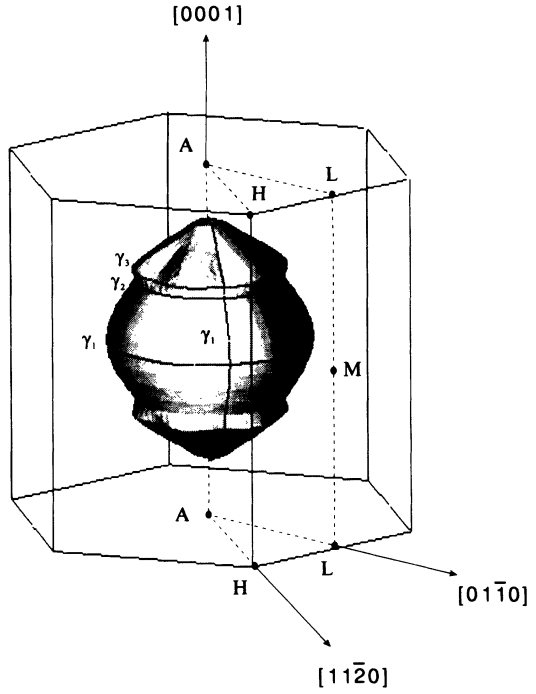

FIG. 8. The football Fermi surface sheet of Pd_2Si with the extremal γ orbits.

are equivalent due to symmetry.[25] We, therefore, compare the theoretical results with experimental data only for the orientation of the magnetic field from [0001] to [11$\bar{2}$0] in the (z,x) plane, between the [11$\bar{2}$0] and the [01$\bar{1}$0] direction in the (x,y) plane, and from [$\bar{1}$100] to [0001] in the (y,z) plane (Fig. 3). As may be seen from Fig. 3, there are three groups of frequencies in this frequency region. The first group is around 500 T, the second group between 1000 T and 1500 T, with very small variation with field direction, and the third group of high frequencies between 3000 T and 6000 T. In order to associate the observed dHvA frequencies with our Fermi surface we have calculated the orientation dependence of the extremal cross section in three symmetry planes us-

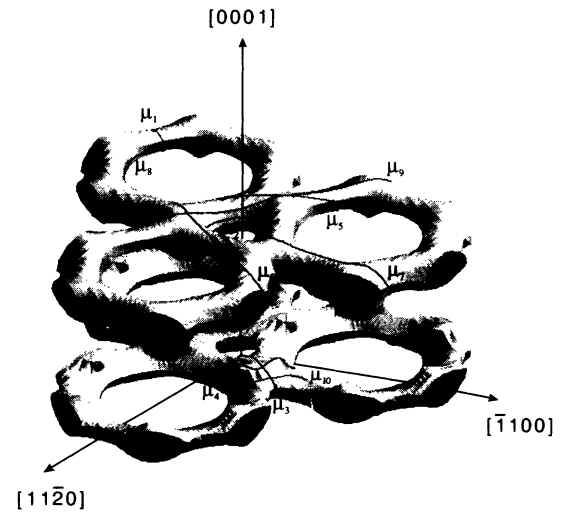

FIG. 7. The rings Fermi surface sheet of Pd_2Si in the extended zone scheme with appropriate extremal μ orbits.

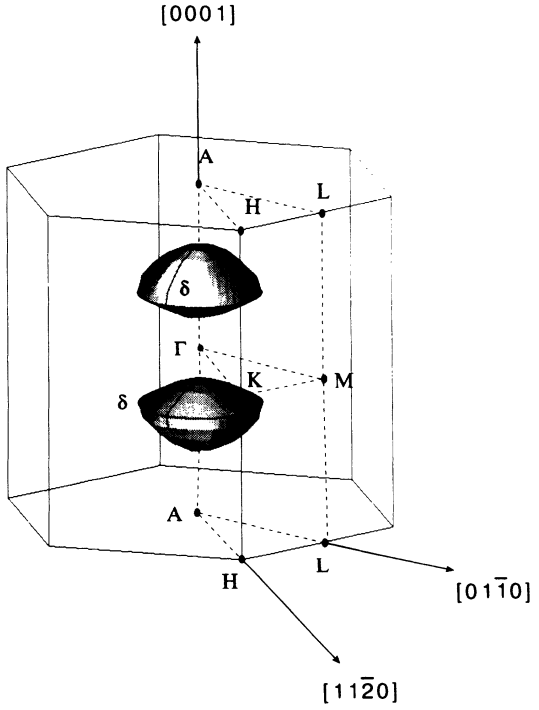

FIG. 9. The *lens* Fermi surface sheet of Pd_2Si with the extremal δ orbit.

ing a 1° step in the magnetic field orientation (Fig. 3). The theoretical and experimental extremal areas of the Fermi surface are compared in Table I for the principal symmetry directions. Theoretically, we have found 17 orbits belonging to different sheets of the Fermi surface. We shall first discuss the simple pieces of Fermi surface, namely, the closed sheets. The smallest orbits labeled α result from the ellipsoid in Fig. 5 and have their minimum near the [0001] direction. We associate this orbit with the lowest experimental branch close to the [0001] direction. The α orbit was not observed experimentally in the whole angular range. It appears near the [0001] direction, in the (z,y) plane and in the $[15° - 40°]$ angle interval, where it decreases with increasing angle. In the (x,y) plane it is not clear which of the three branches should be assigned to the α orbit. The β orbits on the *disk* (Fig. 5) we assign to the third measured branch near the [0001] direction, which has a small negative dispersion going away from the [0001] direction. The ϵ orbits on the *sphere* (Fig. 6) have a very small angular variation and the *sphere* is, therefore, very close to being a sphere. The intermediate size orbits δ result from the *lens* (Fig. 9). We assign the measured branch between 1000 T and 1500 T, showing only small variation with field direction to the δ orbit. This orbit shows the best agreement between experiment and theory. Since the angular dependences of the β and δ oscillations are very similar the *disk* and *lens* have very similar shapes. We assign the highest frequencies observed to the football. There are three extremal orbits on the football. The central γ_1 orbit has been observed in the whole angular range. Even though the absolute discrepancy between the measured and calculated frequencies is large, the angular variation of this orbit is in excellent agreement. Two noncentral orbits γ_2 and γ_3 exist in a small angular range near the [0001] direction. We assign the few measured frequencies around about 2000 T close to the [0001] direction to the γ_2 and γ_3 orbits (the calculated orbits γ_2 and γ_3 nearly coincide).

TABLE I. Theoretical and experimental (Ref. 14) areas of extremal orbits on the Fermi surface of Pd_2Si. In the third column the distance of the cross-section plane from Γ or the symmetry label of the center of the orbit is given.

Orbit	Band	Distance $(2\pi/a)$	Direction	F_{theor} (T)	F_{exp} (T)
α: ellipsoid	h_{35}	A	[0001]	213	386
			$[11\bar{2}0]$	355	555
			$[\bar{1}100]$	352	
β : *disk*	h_{35}	0.472	[0001]	510	508
		0.	$[11\bar{2}0]$	340	422
		0.583	$[\bar{1}100$	430	
ϵ : *sphere*	h_{36}	A	[0001]	608	
			$[11\bar{2}0]$	653	
			$[\bar{1}100]$	644	
μ_1 : rings	h_{36}	0.237	$[11\bar{2}0]$	351	506
		0.	$[\bar{1}100]$	289	
μ_2		0.446	[0001]	393	415
μ_3		0.571	$[\bar{1}100]$	805	
μ_4		0.	$[11\bar{2}0]$	1003	
μ_5		0.3	$[\bar{1}100]$	1192	
μ_6		0.361	$[\bar{1}100]$	2467	
μ_7		0.475	$[\zeta\eta\nu0]$ [a]	3478	
μ_8		0.392	[0001]	3825	
μ_9		0.428	$[\zeta\eta\nu0]$	5476	
μ_{10}		0.073	$[11\bar{2}0]$	469	1164
γ_1 : football		Γ	[0001]	3326	3794
			$[11\bar{2}0]$	5881	5853
			$[\bar{1}100]$	5602	5977
γ_2		0.317	[0001]	1727	1831
γ_3		0.374	[0001]	1756	1992
δ : *lens*	e_{38}	0.316	[0001]	1312	1455
		Γ	$[11\bar{2}0]$	1106	1218
		Γ	$[\bar{1}100]$	1144	

[a] $\zeta = \overline{1.33}$, $\eta = \overline{0.47}$, $\nu = 1.8$.

In addition to the extremal orbits on the closed Fermi surface pieces we have found ten branches of extremal orbits on the rings (Figs. 6 and 7). The orbit with the smallest area, labeled μ_1, results from the neck of the rings (Figs. 6 and 7). With the field in the (x,y) plane we associated this with one of the three experimental branches above it since the angular dependence is the same in this region. The μ_2 orbit is located on the small inner diameter of the rings surrounding the symmetry line H-K (Fig. 7). This orbit exists only close to the [0001] direction. It has the same angular dependence as the second experimental branch for this direction and we therefore assign it to this (Fig. 3). The μ_3, μ_4, μ_5, and μ_{10} group of orbits results from specific aspects of the rings (Fig. 7). The μ_4 and μ_{10} are on the same part of the Fermi surface, but μ_4 is a maximal extremal orbit, and μ_{10} is a minimal extremal orbit. The μ_4 and μ_5 also seem to have been observed since they coincide with several experimental points.

There are some additional orbits on the rings not observed experimentally, namely: μ_6, μ_7, μ_8, and μ_9. The simplest one from the large inner diameter of the rings is labeled μ_8 (Figs. 6 and 7). The μ_7 orbit exists in a very narrow angle range [5°–17°] in the (x,y) plane and the large μ_6 and μ_9 orbits extend over two Brillouin zones (Fig. 7).

Agreement between calculated angular dependence of extremal cross sections and angular variations of the respective dHvA frequencies is rather good for the β and δ orbits in the whole angular interval and for the γ_1 orbit in the (x,y) plane. The calculated γ_2 and γ_3 orbits are somewhat smaller than the measured ones, which is also the case for the γ_1 orbit in the (x,z) plane and around the [0001] direction. The calculated α orbits are also smaller than the observed ones, which is to be expected because of the small size of the ellipsoid and the use of linearly interpolated energy bands between **k** points. The agreement between the observed dHvA frequencies and the calculated ones is quite reasonable for the μ_2, μ_4, and μ_5 orbits. An upward shift of the Fermi energy is necessary to bring the frequency of the electron-type γ orbits closer to the observed values, while a downward shift of the Fermi surface is needed to increase the frequencies of the hole-type μ_1 and μ_3 orbits.

Experimentally, cyclotron masses have been determined for a number of cyclotron orbits, with the magnetic field in the [0001] and the $[11\bar{2}0]$ directions. The resulting

TABLE II. Cyclotron effective masses of Pd_2Si with the magnetic field $B\|[0001]$.

Orbit	$F_{exp}(T)$	$F_{theor}(T)$	m_c^{exp}/m_e	m_c^{theor}/m_e	λ
α	386	213	0.295	0.181	0.630
β	508	510	0.304	0.302	0.007
δ	1455	1312	0.387	0.386	0.003
γ_2	1831	1727	0.474	0.421	0.126
γ_3	1992	1756	0.522	0.422	0.237
γ_1	3784	3326	0.620	0.551	0.125

TABLE III. Cyclotron effective masses of Pd_2Si with the magnetic field $B\|[11\bar{2}0]$.

Orbit	$F_{exp}(T)$	$F_{theor}(T)$	m_c^{exp}/m_e	m_c^{theor}/m_e	λ
β	422	340	0.261	0.260	0.004
μ_1	506	351	0.314	0.271	0.159
α	555	355	0.313	0.211	0.483
μ_{10}	1164	469	0.315	0.260	0.212
δ	1218	1106	0.382	0.281	0.359

masses and comparison with the theoretically calculated ones are given in Tables II and III. No mass determination has been done for the orbits with dHvA frequencies around 6000 T. These orbits had much weaker dHvA signals, presumably due to larger cyclotron masses.

The experimental values of the cyclotron effective masses in these tables are relatively low, ranging from $0.3m_e$ to $0.6m_e$. Much larger values have been calculated from optical reflectivity measurements by Amiotti *et al.*;[12] $m_c^{\|}= 1.1m_e$ and $m_c^{\perp} = 1.8m_e$ for the electric field parallel and perpendicular to the [0001] axis, respectively. This discrepancy can partly be retraced to the simple expression used by these authors to calculate the cyclotron mass, especially to their assumption for the mean free path and of an ellipsoidal Fermi surface. Moreover, the dHvA effect allows direct measurements of the cyclotron mass for each orbit, whereas the masses quoted by Amiotti *et al.*[12] are some average over all orbits. Especially the large high-frequency orbits, whose mass we have not measured, may increase the averaged mass deduced from the optical experiments.

The cyclotron mass m_c^{theor} obtained from band structure theory is related to the experimental mass m_c^{exp} by $m_c^{exp} = m_c^{theor}(1 + \lambda)$, where λ is the orbitally averaged value of the many-body enhancement factor, which contains contributions from electron-phonon and electron-electron interactions. The λ's for the different orbits are also shown in Tables II and III. As may be seen λ varies from being nearly zero for the β and δ orbits to 0.63 for the α orbit.

V. CONCLUSION

On the basis of semirelativistic band structure calculations a model for the Fermi surface of the Pd_2Si is suggested. A reasonable agreement with measured extremal cross sections has been achieved. In addition, some branches of dHvA oscillations associated with orbits on feature 2 have been predicted. It is not possible to obtain closer agreement between predicted and observed values for all orbits simultaneously by shifting the Fermi energy.

ACKNOWLEDGMENTS

One of us (V.N.A.) would like to thank the Max-Planck-Institut für Festkörperforschung for hospitality during his stay in Stuttgart, Germany.

* Present address: National High Magnetic Field Laboratory, Pulsed Field Facility, MS E536, Los Alamos National Laboratory, Los Alamos, NM 87545.

[1] J.T. Lue, Solid State Electron. **26**, 787 (1983).
[2] H. Elabd and W.F. Kosonocky, RCA Rev. **43**, 568 (1982).
[3] J.F. Freeouf, J.W. Rubloff, P.S. Ho, and T.S. Kuan, Phys. Rev. Lett. **43**, 1886 (1979).
[4] A. Franciosi and J.H. Weaver, Phys. Rev. B **27**, 3554 (1983).
[5] G. Rossi, I. Lindau, L. Braicovich, and I. Abbati, Phys. Rev. B **38**, 3031 (1983).
[6] P.S. Ho, G.W. Rubloff, J.E. Lewis, V.L. Moruzzi, and A.R. Williams, Phys. Rev. B **22**, 4784 (1980).
[7] M. De Crescenzi, E. Colavita, U. del Pennino, P. Sassaroli, S. Valeri, C. Rinaldi, L. Sorba, and S. Nannarone, Phys. Rev. B **32**, 612 (1985).
[8] J. Stohr and R. Jaeger, J. Vac. Sci. Technol. **21**, 619 (1982).
[9] S. Nannarone, A.M. Fiorello, U. del Pennino, C. Mariani, M.G. Betti, and M. De Crescenzi, J. Vac. Sci. Technol. A **5**, 1474 (1987).
[10] Juh Tzang Lue, Hong-Wen Chen, and Shwa-Ing Law, Phys. Rev. B **34**, 5438 (1986).
[11] A. Borghesi, G. Guizzetti, L. Nosenzo, A. Piaggi, A. Stella, and G. Majni, Semicond. Sci. Technol. **1**, 184 (1986).
[12] M. Amiotti, G. Guizzetti, F. Marabelli, A. Piaggi, V.N. Antonov, Vl.N. Antonov, O. Jepsen, O.K. Andersen, A. Borghesi, F. Nava, V.V. Nemoshkalenko, R. Madar, and A. Rouault, Phys. Rev. B **45**, 13 285 (1992).
[13] O. Bisi, O. Jepsen, and O.K. Andersen, Phys. Rev. B **36**, 9439 (1987).
[14] E.G. Haanappel, W. Joss, R. Madar, and A. Rouault, Physica B **165&166**, 271 (1990); E.G. Haanappel, Ph.D. thesis, University of Konstanz, 1992.
[15] R. Marani, F. Nava, A. Rouault, R. Madar, and J.P. Senateur, J. Phys. Condens. Matter **1**, 5887 (1989).
[16] N.N. Matyushenko, Poroshk. Metall. **1**, 20 (1964).
[17] C.J. Bradley and A.P. Cracknell, *The Mathematical Theory of Symmetry in Solids* (Clarendon, Oxford, 1972).
[18] O. Laborde, J.C. Lasjaunias, R. Marani, A. Rouault, and

R. Madar, Phys. Rev. B **41,** 9721 (1990).
[19] O. Laborde, U. Gottlieb, and R. Madar (private communication).
[20] D. Shoenberg, *Magnetic Oscillations in Metals* (Cambridge University Press, Cambridge, 1984).
[21] O.K. Andersen, Phys. Rev. B **12**, 3060 (1975).
[22] H.L. Skriver, *The LMTO Method* (Springer, Berlin, 1984).
[23] U. von Barth and L. Hedin, J. Phys. C **4**, 2064 (1971).
[24] O. Jepsen and O.K. Andersen, Solid State Commun. **9**, 1763 (1971).
[25] M. Lax, *Symmetry Principles in Solid State and Molecular Physics* (Wiley, New York, 1974).

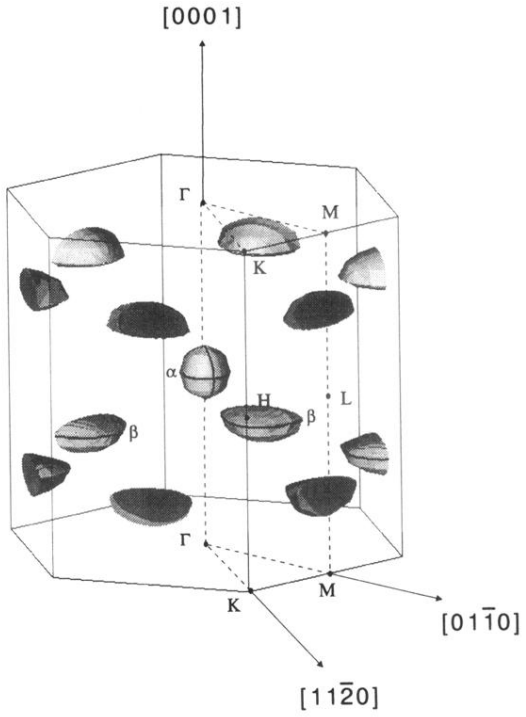

FIG. 5. The Fermi surface sheet, the ellipsoid, around the *A* point and the *disk* sheet in the first Brillouin zone. Greek letters denote extremal orbits on the Fermi surface of Pd_2Si.

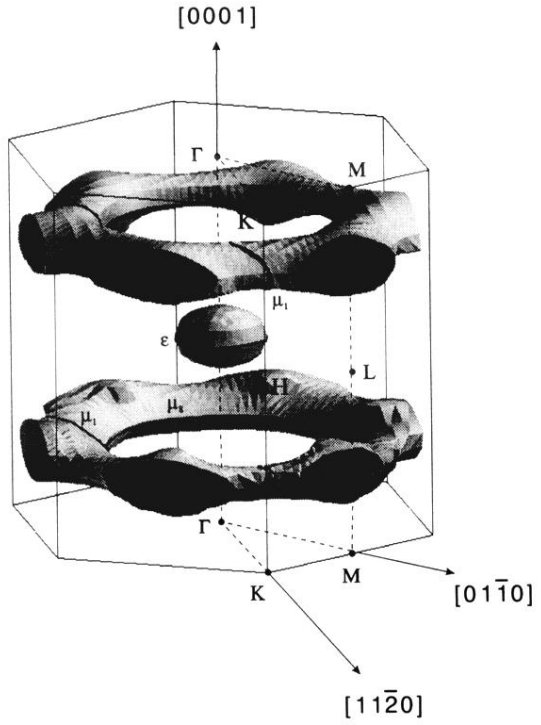

FIG. 6. The rings and the *sphere* Fermi surface sheets of Pd_2Si in the first Brillouin zone. ϵ, μ_1, and μ_8 are extremal orbits.

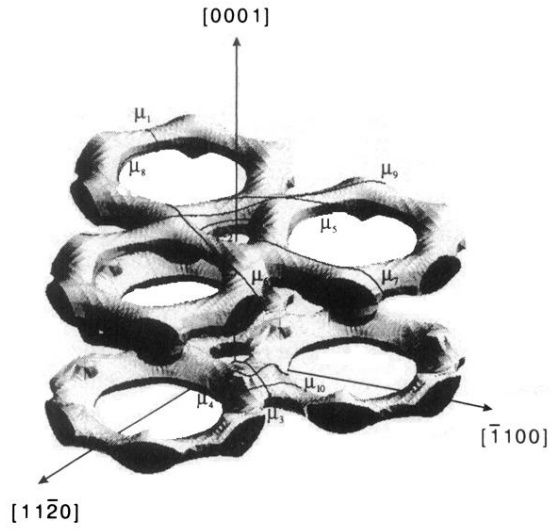

FIG. 7. The rings Fermi surface sheet of Pd_2Si in the extended zone scheme with appropriate extremal μ orbits.

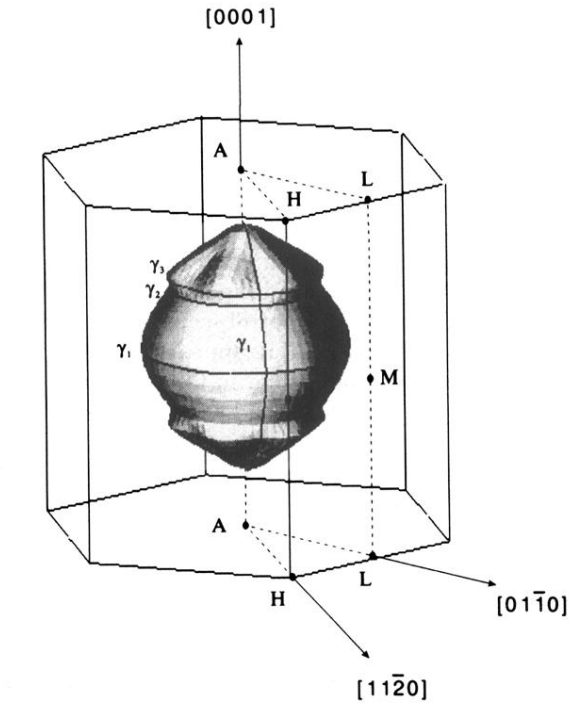

FIG. 8. The football Fermi surface sheet of Pd_2Si with the extremal γ orbits.

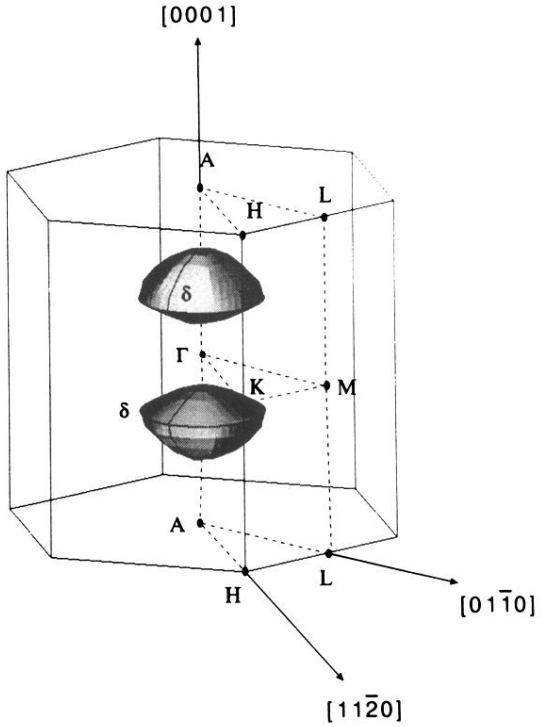

FIG. 9. The *lens* Fermi surface sheet of Pd_2Si with the extremal δ orbit.